NASA/CR—1998- 208201

Radiation Monitoring Devices, Inc.
44 Hunt Street
Watertown, MA 02172

STUDIES OF AVALANCHE PHOTODIODES (APDS) AS READOUT DEVICES FOR SCINTILLATING FIBERS FOR HIGH ENERGY GAMMA-RAY ASTRONOMY TELESCOPES

TECHNICAL PROGRESS REPORT
Period of Performance: January 16, 1998 – May 15, 1998

By:
STEFAN VASILE, PH.D.
SUZANNE SHERA, M.S.
DENIS SHAMO, B.S.

RMD, Inc. Watertown, MA

Submitted to:
NASA, George C. Marshall Space Flight Center
Huntsville, Alabama 35812
Grant # NASA H-29453D

I. INTRODUCTION

New gamma ray and charged particle telescope designs based on scintillating fiber arrays could provide low cost, high resolution, lightweight, very large area and multi radiation length instrumentation for planned NASA space exploration. The scintillating fibers low visible light output requires readout sensors with single photon detection sensitivity and low noise. The sensitivity of silicon Avalanche Photodiodes (APDs) matches well the spectral output of the scintillating fibers. Moreover, APDs have demonstrated single photon capability.

The global aim of our work is to make available to NASA a novel optical detector concept to be used as scintillating fiber readouts and meeting the requirements of the new generations of space-borne gamma ray telescopes.

We proposed to evaluate the feasibility of using RMD's small area APDs (μAPD) as scintillating fiber readouts and to study possible alternative μAPD array configurations for space borne readout scintillating fiber systems, requiring several hundred thousand to one million channels. The evaluation has been conducted in accordance with the task description and technical specifications detailed in the NASA solicitation "Studies of Avalanche Photodiodes (APDs) as readout devices for scintillating fibers for High Energy Gamma-Ray Astronomy Telescopes" (# 8-W-7-ES-13672NAIS) posted on October 23, 1997.

The feasibility study we propose builds on recent developments of silicon μAPD arrays and light concentrators advances at RMD, Inc. and on more than 5 years of expertise in scintillating fiber detectors. In a previous program we carried out the initial research to develop a high resolution, small pixel, solid-state, silicon APD array which exhibited very high sensitivity in the UV-VIS spectrum. This μAPD array is operated in Geiger mode and results in high gain ($>10^8$), extremely low noise, single photon detection capability, low quiescent power (less than 10 μW/pixel for 30 μm sensitive area diameter) and output in the 1-5 volt range.

If successful, this feasibility study will make possible the development of a scintillating fiber detector with unsurpassed sensitivity, extremely low power usage, a crucial factor of merit for space based sensors and telescopes.

II. PROPOSED CONCEPT AND ANALYSIS METHOD DESCRIPTION

We proposed to evaluate the feasibility of a novel optical detector array for scintillating fiber array readouts based on our μAPD array technology. The detector array will use the μAPD array technology in conjunction with an integrated optical concentrator array, which interfaces with the scintillating fibers. The concentrator array will be aligned and cemented to the sensitive area of the μAPD pixels. The concentrator array pitch and input aperture will be designed to match the scintillating fiber size required by the application. This concept promises to preserve the advantages of the μAPD design (small area, low dark count rate) while increasing the optical signal level available for detection through the use of concentrators.

Our analysis approach is to evaluate the tradeoffs between the concentrator light transfer efficiency and μAPD area while maintaining a high detection efficiency and low quiescent power of the composite *APD – concentrator* detector.

III. TECHNICAL OBJECTIVES

The project tasks address the evaluation of the μAPD and optical interfacing device performance based on existing μAPD devices and fabricated concentrator prototypes. The goal is to assess the feasibility of using Geiger mode, passively quenched, μAPD arrays with integrated concentrators as scintillating fiber readouts for the specific application, and to evaluate the opportunity of continued research leading to the integration of avalanche photodiode arrays into large area gamma ray telescopes. The tasks of the project are:

- Determine the feasibility and operating characteristics of arrays of APDs used in the Geiger mode for the readout of scintillation pulses from plastic fibers with the specified characteristics;
- Estimate the μAPD significant characteristics for the application and identify tradeoffs;
- Study possible alternative configurations for array sizes and pitch and their effect on the above characteristics to optimize the use of APDs for space-borne readout of scintillating fiber systems of several hundred thousand to one million channels.

IV. ACCOMPLISHED TECHNICAL OBJECTIVES

TASK 2: ESTIMATE THE APD SIGNIFICANT CHARACTERISTICS AND IDENTIFY TRADEOFFS

During the first 4 months, we evaluated the following issues related to the μAPD performance:

- Recovery time for different passive quenching configurations;
- Extrapolation of the measured dark count rate data to the expected μAPD sensitive area range and temperature;
- The detection efficiency for 30 μm μAPD pixel size.

2.1. Recovery time for different passive quenching configurations.

We estimate that APDs with more than 30μm diameter will be the candidates for the scintillating array high sensitivity low power optical detector. Therefore, we evaluated the timing performance (recovery time) for 30 μm diameter APDs. (APDs with 150 – 300 μm diameter have been designed and are currently in the fabrication phase). The recovery time, defined as the total Geiger pulse width at 10% peak value, was measured for standard passive quenching mode and active load quenching. The active load quenching circuit uses a high speed (f_t= 2 GHz) **npn** bipolar transistor to amplify the Geiger current and to initiate early quenching of the avalanche, through the emitter limiting resistor load. The transistor is biased at 5 volts. The measured reset time and the energy/Geiger pulse vs the active load resistor, are shown in **Table 1.** The recorded Geiger pulse shapes for 20 and 1 kΩ active load resistors are shown in **Figures 1(a)** and **(b).**

Mode	Load Resistance	Recovery Time	Peak Current	Energy/ pulse	Quiescent Power @ 100 counts/sec
	KΩ	μsec	mA	nJ	μW
Passive quenching	100	20	0.03	1.5	0.2
Active Load Quenching	20	14	0.2	5.1	0.5
Active Load Quenching	6	4.0	0.5	4.8	0.5
Active Load Quenching	3	1.8	1.1	4.7	0.5
Active Load Quenching	1	0.9	3.4	7.0	0.7
Active Load Quenching	0.5	0.5	6.1	7.0	0.7

Table 1. The measured recovery time and energy/pulse on 30 μm diameter μAPDs for passive and active load quenching. The use of active load quenching improves the recovery time to 0.9 μsec, for 1 KΩ active resistor load. All the measurements were taken at 3.5 volts above the breakdown voltage, except for the 0.5KΩ load (due to low voltage drop on the resistive load, the allowed applied bias was only 3 volts above the breakdown voltage). Further selection of the bipolar transistor (higher *hfe*) would allow biasing the μAPD at the nominal voltage above breakdown (3.5-4 volts) while maintaining low recovery time. The quiescent power peaks in the 0.7 μW range and would require only a fraction of the power planned for the GLAST/ tracker modules. Recovery times shorter than 1 μsec meet the proposal technical specifications for GLAST.

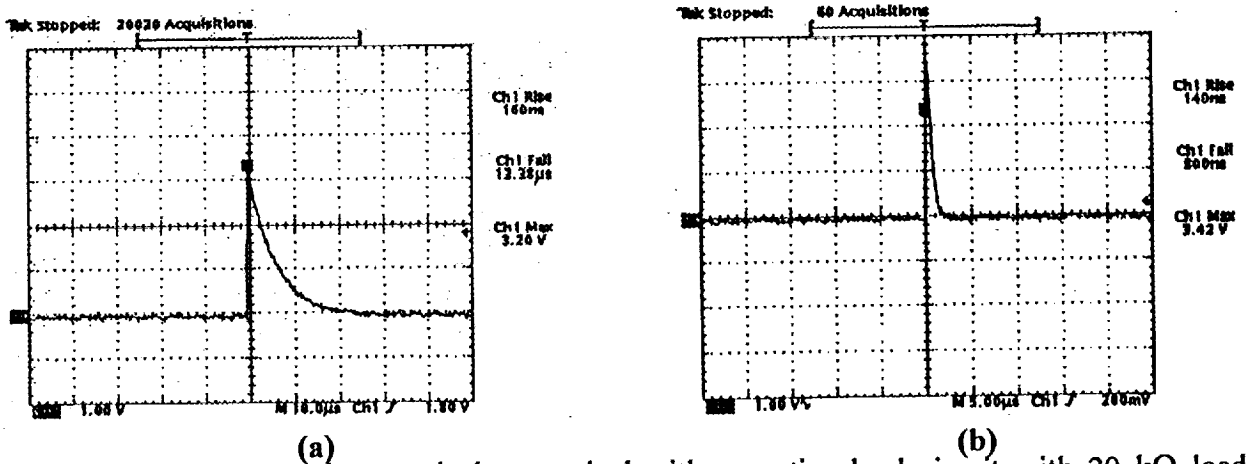

(a) (b)

Figure 1 (a). Geiger pulse, passively quenched with an active load circuit with 20 kΩ load resistors; **(b)** Passively quenched pulse with 1 KΩ active load resistors. The recovery time is 940 nsec, and meets the timing specifications.

2.2. Extrapolation of the measured dark count rate data to the expected APD sensitive area range and temperature.

One important question we have to answer is how to accurately predict the maximum μAPD sensitive area and the operating temperature resulting in less than 100 Hz dark count rate, using measurements on existing APDs. In order to predict the dark count rate dependence on temperature at different bias, we measured the dark count rate on 30 μm APDs over a wide temperature range and evaluated the activation energy for different applied bias voltages. The extrapolation of the dark count rate at lower temperatures is shown in **Figure 2** and will be the basis for the evaluation of the required operating temperature for a particular μAPD area.

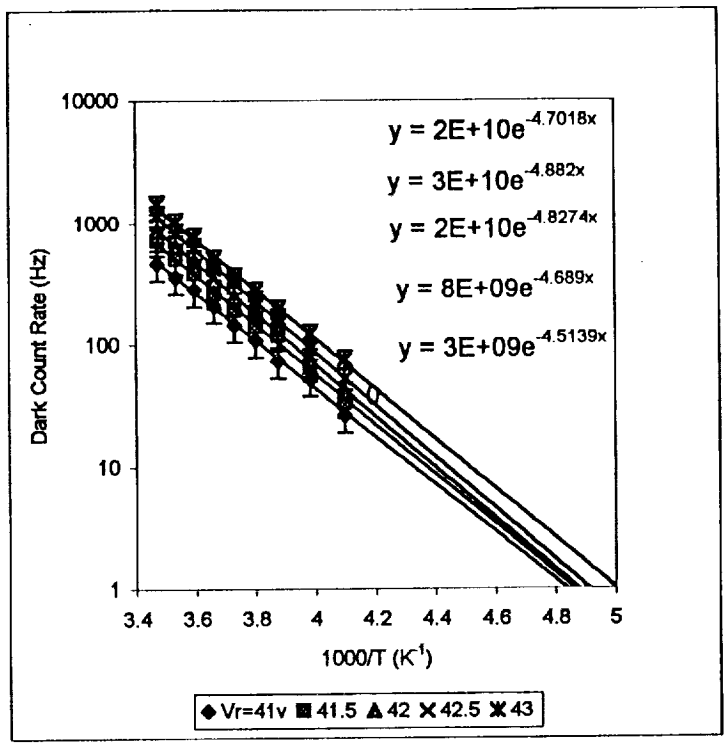

Figure 2. Measured and predicted dependence of the dark count rate on temperature for 30 μm diameter μAPD. Inserts show the fitted analytical functions associated with each applied voltage. These functions will be used to predict the overall μAPD performance.

2.3. Detection Efficiency

The detection efficiency was tested with pulsed LEDs emitting at 470 nm peak wavelength. Lenses were used to spread out the light spot to approximately 14 mm diameter. Light uniformity was tested prior to the detection efficiency measurements. The LED was pulsed for 50 msec and the light spot was imaged with a Photometrix cooled CCD camera (flat field correction was used to factor in the camera non-uniformity). The light spot uniformity was better than 3% over 10 mm diameter apertures.

For the detection efficiency measurement, the LED was biased with approximately 100 nsec current pulses at 1 kHz repetition frequency. The number of photons/pulse was adjusted by modifying the LED driver pulse width. The photon density was calibrated using a Hamamatsu Si photodiode with 6 mm diameter of the sensitive area. The detection efficiency dependence on bias is shown in **Figure 3** for a low number of photons/pulse incident on the avalanche region. The detection efficiency increases monotonically with the number of photons/pulse and reaches 98% at 12 photons/pulse.

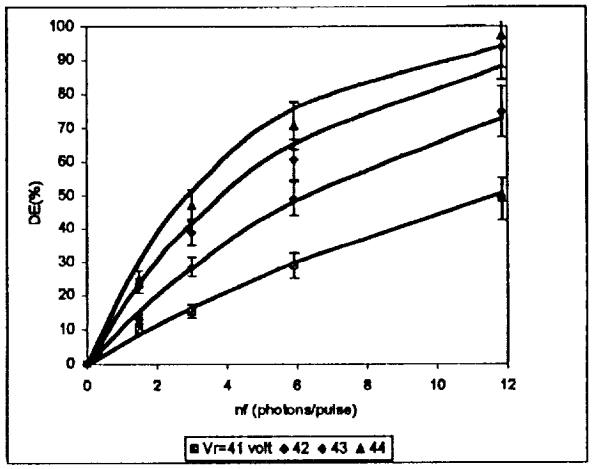

Figure 3. μAPD detection efficiency versus the number of photons, n_f, incident on the sensitive area.

The data were fitted to the detection efficiency equation $DE = 1 - \exp(-P_b \cdot QE \cdot n_f)$, where DE is the detection efficiency, P_b x QE is the is the product of *breakdown probability* and *quantum efficiency*, and n_f is the number of photons / pulse. The analytical expression will be used to evaluate the tradeoffs between sensitivity, speed and quiescent power (noise).

TASK 3: STUDY POSSIBLE ALTERNATIVE CONFIGURATIONS

We planed to investigate two classes of concentrators, namely cone and aspheric mirror concentrators. The goals are: (1) to predict the performance of these concentrators; (2) to select a design ready to be prototyped and to be integrated into a single pixel μAPD detector, and (3) to identify next generation high efficiency concentrator array designs.

3.1 Cone Concentrators

During this period we evaluated analytically the maximum concentration factor of cone concentrators, fabricated a few cone concentrator prototypes and measured the light concentration efficiency for different concentration ratios. **Figure 4** shows the schematic of a mirror cone concentrator coupled to a scintillating fiber of diameter D_f. The cone has the entrance face diameter D_{in}, exit face diameter D_{out}, (usually matching the μAPD active area diameter), and the light acceptance angle $\alpha_{acceptance}$.

For a cone concentrator the concentration factor, CF, is defined as the ratio of areas of the entrance and exit faces:

$$CF = \frac{(D_{in})^2}{(D_{out})^2}$$

In such a concentrator, the angle of incidence of an incident ray of light changes on successive reflections. In order for such a ray to reach the exit face and not be back-reflected, the following condition must be obeyed:

$$\alpha_{acceptance} = \arcsin\left(\frac{1}{\sqrt{CF} + \frac{\frac{D_f^{\,2}}{4}\cdot\sqrt{CF} - \frac{D_f}{2}\sqrt{\frac{D_f^{\,2}}{4} + L^2 - \frac{L^2}{CF}}}{\frac{D_f^{\,2}}{4} - \frac{L^2}{CF}}}\right)$$

where L represents the distance between the entrance face and the cone apex. All the rays incoming at an angle lesser or equal to $\alpha_{acceptance}$ will be conveyed to the exit face. **Figure 5** shows the relationship between the maximum acceptance angle, and the concentration factor for a cone concentrator of 20 mm length.

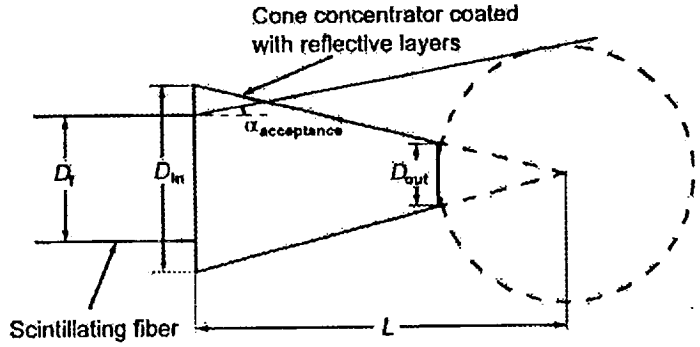

Figure 4. Schematic of the mirror cone concentrator with a scintillating fiber coupled to the entrance aperture. The dashed circle represents a hypothetical line, defining the boundary outside of which the incident rays will be back-reflected to the concentrator entrance. The line tangent to the circle defines the maximum acceptance angle, $\alpha_{acceptance}$, of the cone concentrator.

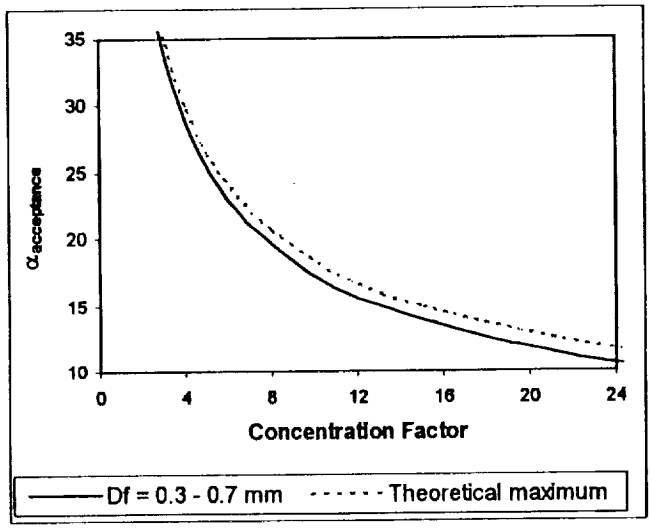

Figure 5. The acceptance angle versus the concentration factor. For high concentration factors the acceptance angle will be less than the incident angle of the rays emitted by the scintillating fiber, and consequently some light losses will occur due to back-reflection.

We fabricated cone concentrators with 1mm diameter input aperture and various exit aperture diameters. The cone concentrators were spliced with 1 mm Bicron, BCF 20, single-cladding scintillating fibers emitting green photons. The conic surface was coated with Al. The scintillating fiber was excited with a UV lamp, and the light output at the cone concentrator exit surface was monitored with a 1.2 mm diameter active area photodiode, coupled to the concentrator via an index matching optical fluid. **Figure 6** shows the measured concentration efficiency for different concentration factors.

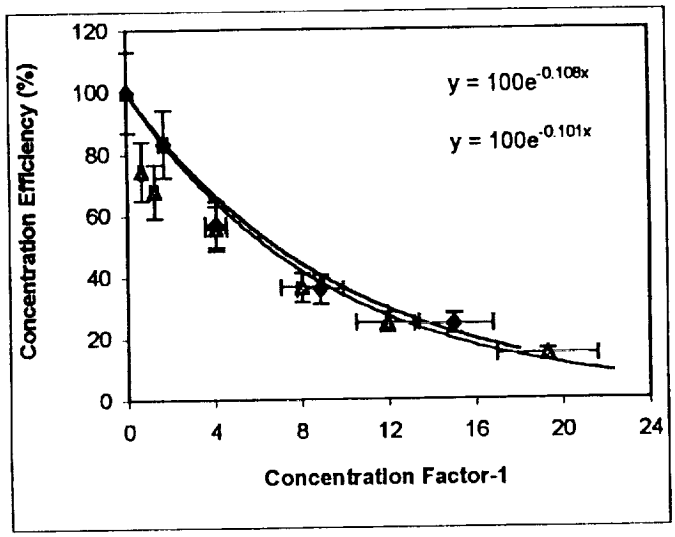

Figure 6. Measured concentration efficiency for two prototype cone micro-concentrators designed and fabricated at RMD Inc. The results show good repeatability of the concentrating efficiency. The concentration efficiency for 16:1 concentration factors (24%) is in good agreement with the previous results measured on large concentrators (26%).

3.2 Aspheric Mirror Concentrators

The cone mirror concentrator design has limited light collection efficiency capability at high concentration factors, and does not allow a compact concentrator design. Aspheric mirror concentrators can overcome this problem. Multi-parametric polynomial optimization of these mirrors can increase the optimization procedure flexibility and should result in increased concentration efficiency as compared to cone concentrators.

Ray tracing was used to predict the performance of aspheric mirror concentrators. We evaluated the concentration efficiency, assuming scintillating fibers with NA =0.66 spliced to a quartz mirror concentrator and plotted the results in **Figure 7a**.

Recently we have processed such a mirror concentrator using 200 μm diameter silica fibers (see micrograph in **Figure 7b**). The mirror concentrator was laser machined at one end and the meniscus surface was deposited with a reflecting film. The fiber tip was subsequently polished to create the exit aperture of the mirror. Currently we are fabricating the mirror aspheric concentrators with 500 μm input aperture diameter, and we plan to test their performance by the end of May.

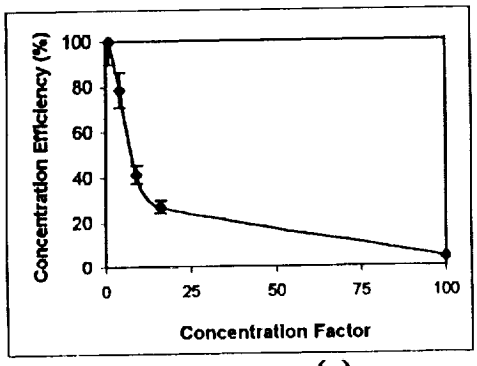

(a)

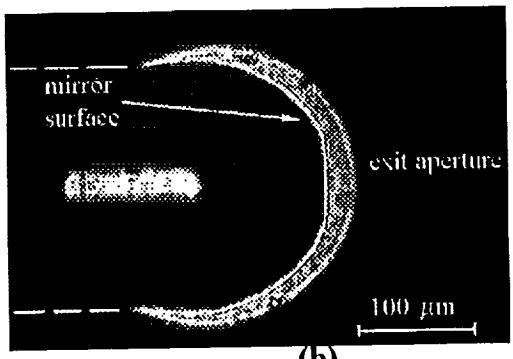

(b)

Figure 7(a). Ray tracing results for an aspheric concentrator versus the concentration factor for a scintillating fiber with NA=0.66. As compared to the cone concentrators, the parabolic concentrators yield higher concentration efficiencies for concentration factors greater than 25; **(b)** Micrograph of the experimental micro-mirror concentrator. The silica fiber end was laser machined to the desired shape and aluminum was subsequently deposited. The mirror end was polished. Such mirror arrays will be cemented together and aligned to the μAPD array to result in a rugged, high sensitivity optical detector.

TASK 1: DETERMINE THE FEASIBILITY AND OPERATING CHARACTERISTICS OF APD ARRAYS

Based on the measured performance of the μAPD arrays and cone concentrators, we generated the analytical functions necessary to evaluate the overall performance of the integrated *APD-concentrator* array. The room temperature detection efficiency was calculated for two bias voltages (42 and 43 volts), with the diameter of the scintillating fiber as a parameter. Single cladding and double cladding scintillating fibers with 8,000 photons/MeV scintillation yield, and 3.5 m attenuation length, were assumed as light sources for the *concentrator - μAPD* detector assembly performance predictions. The results are summarized in **Figures 8-13.**

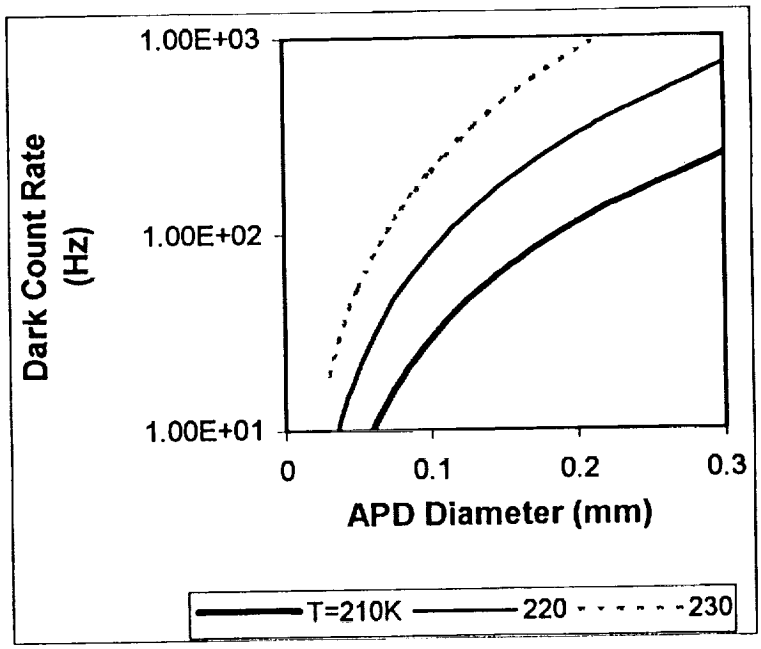

Figure 8. Predicted μAPD dark count rate versus the μAPD diameter at 2 volts applied bias above the breakdown voltage for three operating temperatures.

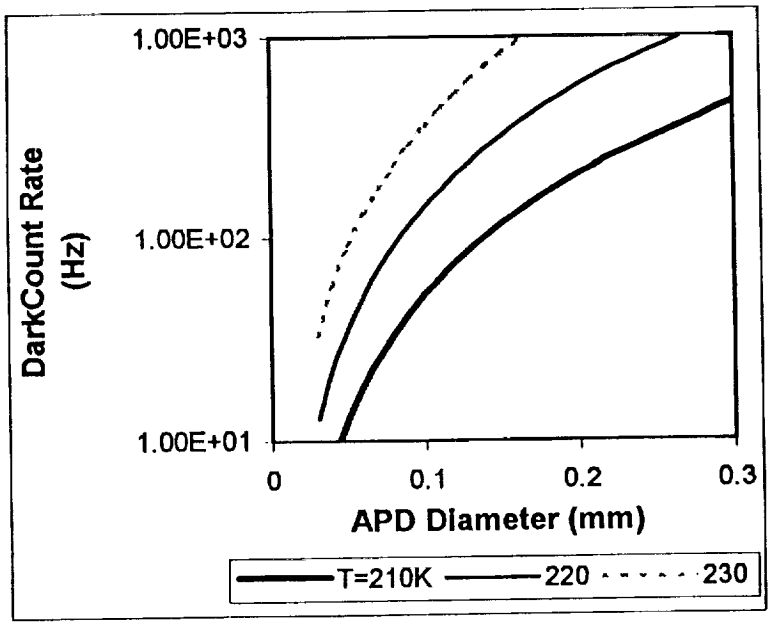

Figure 9. Predicted μAPD dark count rate versus the μAPD diameter at 3 volts applied bias above the breakdown voltage for three operating temperatures.

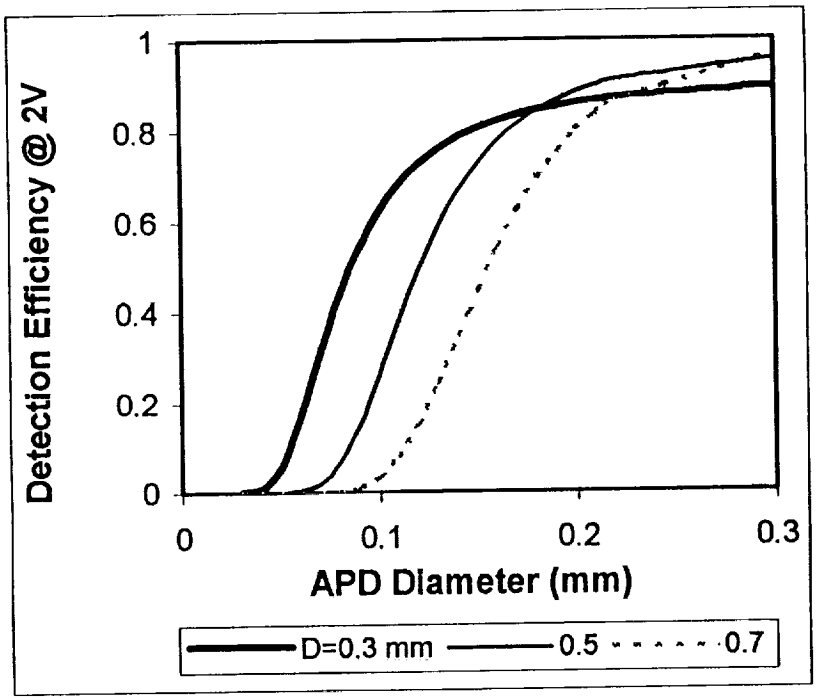

Figure 10. Predicted upper limit of the *concentrator– μAPD* detection efficiency for 0.3, 0.5 and 0.7 mm diameter double cladding scintillating fibers, at 42 volts applied bias (5.6% scintillation trapping efficiency was assumed for double cladding fibers).

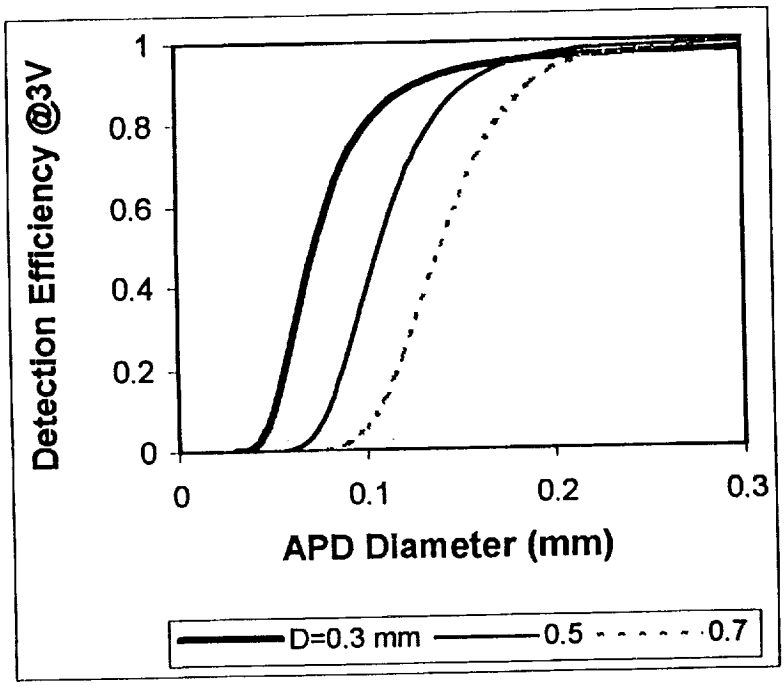

Figure 11. Predicted upper limit of the *concentrator– μAPD* detection efficiency for 0.3, 0.5 and 0.7 mm diameter double cladding scintillating fibers, at 43 volts applied bias (5.6% scintillation trapping efficiency was assumed for double cladding fibers).

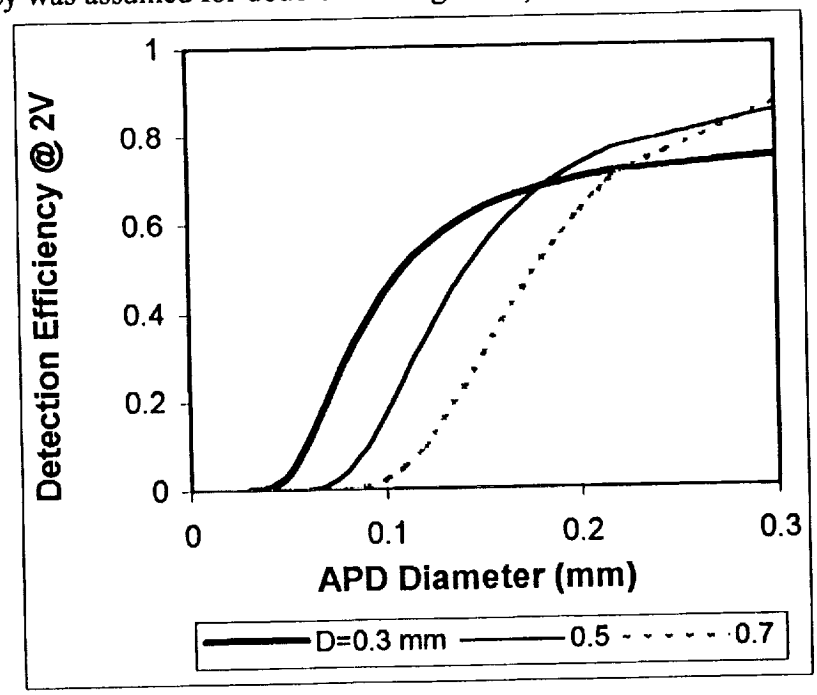

Figure 12. Predicted lower limit of the *concentrator– μAPD* detection efficiency for 0.3, 0.5 and 0.7 mm diameter single cladding scintillating fibers, at 42 volts applied bias (3.4% scintillation trapping efficiency was assumed for single cladding fibers).

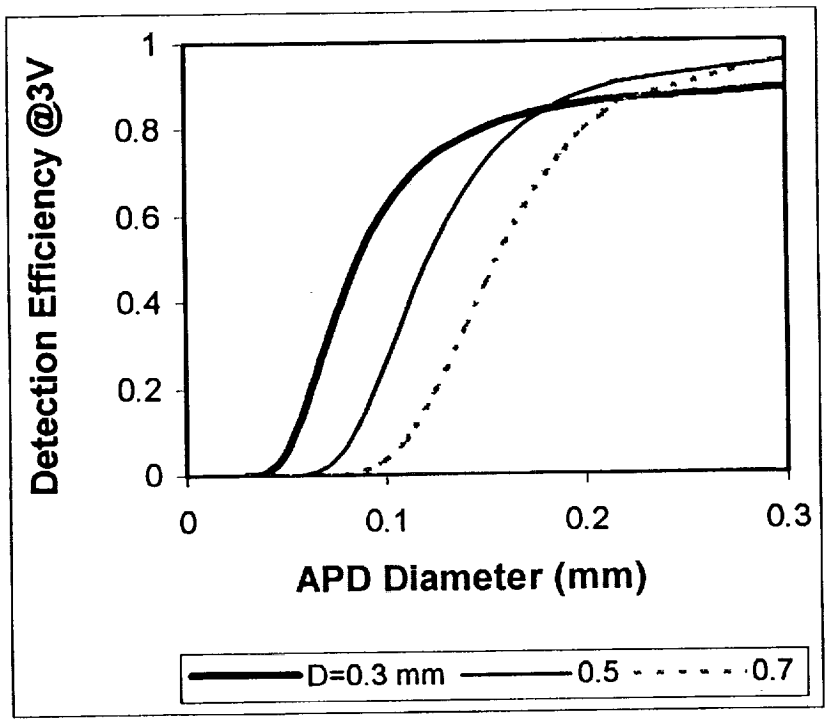

Figure 13. Predicted lower limit of the *concentrator– μAPD* detection efficiency for 0.3, 0.5 and 0.7 mm diameter single cladding scintillating fibers, at 43 volts applied bias (3.4% scintillation trapping efficiency was assumed for single cladding fibers).

INTERIM CONCLUSIONS

The conclusions on the study of conceptual performance limitations for the fiber readout application are:

1. Cone concentrators with simple, and potentially low cost fabrication technology, resulted in decreased μAPD area and consequently lower dark count rate, without inducing significant limitations of the detection efficiency;
2. There is an μAPD diameter threshold required to operate the integrated *concentrator-μAPD* detector at high detection efficiency;
3. Fibers ranging from 0.3 to 0.7 mm can be efficiently read out by the integrated detectors;
4. Passive quenching with active load allows to decrease the recovery time to 1 μsec at only 0.7 μW quiescent power at 100 Hz dark count rate;
5. Cooling to 220 K is required to meet the dark count rate condition (100 Hz) for 0.5 mm diameter scintillating fibers. We want to point out that the dark count rate limitation is not purely conceptual: further μAPD fabrication process improvement may decrease the leakage currents and consequently reduce the dark count rate;
6. Shorter recovery times would permit faster gating settings, and would allow tolerating higher dark count rates.